NANO LETTERS

LETTER

pubs.acs.org/NanoLett

Circularly Symmetric Light Scattering from Nanoplasmonic Spirals

Jacob Trevino,[†] Hui Cao,[‡] and Luca Dal Negro*[,†,§]

[†]Division of Materials Science and Engineering, Boston University, 15 Saint Mary's Street, Brookline, Massachusetts 02446, United States

[‡]Department of Applied Physics, Yale University, New Haven, Connecticut 06520-8482, United States

[§]Department of Electrical and Computer Engineering and Photonics Center, Boston University, 8 Saint Mary's Street, Boston, Massachusetts 02215, United States

Supporting Information

ABSTRACT: In this paper, we combine experimental dark-field imaging, scattering, and fluorescence spectroscopy with rigorous electrodynamics calculations in order to investigate light scattering from planar arrays of Au nanoparticles arranged in aperiodic spirals with diffuse, circularly symmetric Fourier space. In particular, by studying the three main types of Vogel's spirals fabricated by electron-beam lithography on quartz substrates, we demonstrate polarization-insensitive planar light diffraction in the visible spectral range. Moreover, by combining dark-field imaging with analytical multiparticle calculations in the framework of the generalized Mie theory, we show that plasmonic spirals support distinctive structural resonances with circular symmetry carrying orbital angular momentum. The engineering of light scattering phenomena in deterministic structures with circular Fourier space provides a novel strategy for the realization of optical devices that fully leverage on enhanced, polarization-insensitive light-matter coupling over planar surfaces, such as thin-film plasmonic solar cells, plasmonic polarization devices, and optical biosensors.

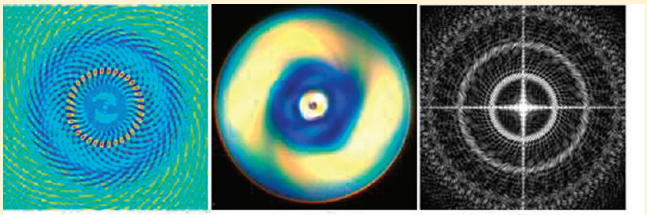

KEYWORDS: Aperiodic structures, plasmonics, surface plasmons, optical quasicrystals

Recent advancements in the design and fabrication of deterministic aperiodic nanostructures (DANS) have provided novel opportunities for the creation and manipulation of complex scattering resonances and nanoscale localized optical fields.[1−3] DANS are inhomogeneous metal-dielectric structures in which the refractive index fluctuates over multiple length scales comparable or smaller than the wavelength of light. These structures are designed by mathematical rules, which interpolate in a tunable fashion between periodicity and randomness.[2−6] In particular, their reciprocal Fourier space (i.e., Fraunhofer diffraction pattern) ranges from a discrete set of δ-like Bragg peaks (i.e., pure-point spectrum), such as for periodic and quasiperiodic crystals, to a continuous spectrum (i.e., absence of Bragg peaks), as encountered in amorphous systems.[3,5−7] Moreover, because of a far richer structural complexity compared to periodic, quasiperiodic, and disordered random media, the Fourier space of DANS can encode noncrystallographic point-symmetries with rotational axes of arbitrary order.[8−13]

On the other hand, disordered and amorphous structures are characterized by diffuse Fourier spectra that can support continuous rotational symmetry (i.e., circular symmetry of scattering rings).[7,14,15] Only recently, deterministic structures with infinite-order rotational symmetry, or circular symmetry, in reciprocal (i.e., Fourier) space have been constructed by a simple procedure that iteratively decomposes a triangle into five congruent copies.[8] The resulting aperiodic tiling, named the Pinwheel tiling, has triangular elements (i.e., tiles) that appear in infinitely many orientations. Its diffraction pattern approximates continuous circular symmetry in the limit of an infinite-size structure.[8] Here we will show that finite-size particle arrays with continuous circular symmetry in Fourier space can also be obtained by engineering aperiodic spiral order.

In this paper, by combining experimental dark-field microimaging, spectroscopy and rigorous multiple scattering calculations based on the generalized Mie theory (GMT),[3,16−20] we investigate the light scattering properties of plasmonic DANS with continuous and circularly symmetric Fourier space. Specifically, we will focus on the three main types of Vogel's spirals, which lack both translational and orientational symmetry in real space while displaying continuous circular symmetry in reciprocal space.[21−23] Differently from the most commonly investigated aperiodic structures, the Fourier space of Vogel's spirals consists of continuous scattering rings, similarly to the electron diffraction patterns observed in amorphous solids and liquids, or more generally in hyperuniform point patterns.[14] Despite that no rigorous results exist on the spectral properties of aperiodic spirals, they appear to exemplify the fascinating concept, introduced by Ruelle, of "turbulent crystals" characterized

Received: January 31, 2011
Revised: March 28, 2011

dx.doi.org/10.1021/nl2003736 | *Nano Lett.* XXXX, XXX, 000–000

by long-range order, group symmetries (such as rotations), and continuous spectra.[24]

Recently, the concept of aperiodic spiral order has been investigated in the context of dielectric structures, such as photonic crystal fibers, where it led to the demonstration of large birefringence with tunable dispersion.[25−27] Moreover, large and omnidirectional photonic bandgaps were theoretically predicted for sunflower spiral arrays of dielectric rods.[28] In our paper, we will systematically investigate light scattering from different types of plasmonic Vogel's spirals of Au nanoparticle arrays fabricated by electron beam lithography (EBL) on transparent quartz substrates. By performing dark-field scattering microscopy in partnership with GMT calculations, we will experimentally demonstrate polarization-insensitive circular diffraction and planar scattering in aperiodic spirals and we will engineer circular scattering versus the characteristic geometric parameters of the structures. In this paper, we will focus on the radiative (i.e., diffractive) coupling regime, which is responsible for the formation of distinctive structural resonances carrying orbital angular momentum in the scattered radiation from aperiodic spirals. In addition to its fundamental interest, the study of DANS with circular Fourier space provides access to the engineering of nanostructures giving rise to polarization-insensitive planar diffraction effects over large frequency bandwidths, suggesting a number of device applications such as compact circular polarization devices, optical biosensors, and enhanced thin-film solar cells.

Vogel's Spiral Arrays. Vogel's spirals can be considered a subset of the more general class of Fermat's spirals. They are obtained by a simple generation rule, expressed in polar coordinates r and θ, first proposed by Vogel in order to approximate in two spatial dimensions the complex arrangements of florets in the sunflower head[21−23]

$$r = a\sqrt{n} \tag{1}$$

$$\theta = n\alpha \tag{2}$$

where $n = 0, 1, 2,...$ is an integer, a is a constant scaling factor, $\alpha \approx 137.508°$ is an irrational number known as the "golden angle" that can be expressed as $\alpha = 360/\varphi^2$, where $\varphi = [1 + (5)^{1/2}]/2 \approx 1.618$ is the golden number, which can be approximated by the ratio of consecutive Fibonacci numbers. Rational approximations to the golden angle can be obtained by the formula $\alpha° = 360 \times (1 + p/q)^{-1}$ where p and $q < p$ are consecutive Fibonacci numbers. The angle α gives the constant aperture between adjacent position vectors $r(n)$ and $r(n + 1)$ of particles in the "sunflower spiral", also called the "golden spiral", and here referred to as the g-spiral. The structure of a g-spiral can be decomposed into an equal number of clockwise and counterclockwise spiral families originating from its center. The number of spirals in each family is found to be a Fibonacci number. Additionally, since the golden angle is an irrational number, the g-spiral lacks both translational and rotational symmetry. Accordingly, its spatial Fourier spectrum does not exhibit well-defined Bragg peaks, as for standard photonic crystals and quasicrystals, but shows diffuse circular rings. The g-spiral has been investigated by both biologists and mathematicians for many centuries.[21−23,29] This pattern is frequently encountered in the spatial arrangement of leaves, bracts, and florets, most notably as in the seeds of a sunflower.[29] Vogel's spirals with remarkably different structures can be obtained by choosing only slightly different values for the aperture angle α, thus providing the opportunity to simply control and explore distinctively different degrees of aperiodic structural complexity.

In this study, we will focus on the three most investigated types of aperiodic spirals, which include the g-spiral and two other aperiodic spirals obtained by the following choice of divergence angles: $\alpha_1 = 137.3°$ (i.e., α_1-spiral) and $\alpha_2 = 137.6°$ (i.e., α_2-spiral), respectively.[29] The α_1 and α_2-spirals are called "nearly golden spirals", and their families of diverging arms, known as parastichies, are considerably fewer. It is the case when the divergence angle is slightly less than the golden angle, as for the α_1-spiral, gaps appear in the center head of the spiral, and only the clockwise family of spiral arms can be seen. Gaps appear again if the divergence angle is slightly larger than the golden angle, as for the α_2-spiral, but this time only the counterclockwise family of spiral arms can be appreciated.[29] The g-spiral is the only structure where the two spiral families are uniformly interlocked and the particles pack closely together without gaps.

Fabrication of Plasmonic Vogel's Spiral Arrays. The nanoparticle spiral arrays were fabricated using EBL on quartz substrates. As detailed elsewhere,[3] our fabrication process flow starts with 180 nm of PMMA 950 (poly(methyl methacrylate)) spin coated on top of the substrate, followed by a soft bake at 180 °C for 20 min. The nanopatterns were written using a Zeiss SUPRA 40VP SEM equipped with Raith beam blanker and NPGS for nanopatterning. After developing the resist in MIBK (methylisobutyle ketone), a thin metal stack was deposited on the patterned surface by electron-beam evaporation. The stack consisted of a 2 nm Cr adhesion layer followed by a 23 nm Au layer. The lift-off process was performed using heated acetone. The fabricated types of Au nanoparticle spirals are shown in the scanning electron micrographs (SEM) of Figure 1a−f. All the metal particles are cylindrical in shape with a circular diameter of 200 nm and thickness of 30 nm. Following the described procedure, for each spiral type we fabricated a set of samples with varying minimum interparticle separation (edge-to-edge), ranging between 90 and 680 nm and number of particles ranging between 8000 and 33 058. This effort enabled a systematic study of the influence of the array geometry and dimensionality on the scattering properties. All the arrays have been spaced on the chip by approximately 300 μm in order to avoid undesired cross talk.

Fourier Space Analysis. In order to better understand the diffraction properties of plasmonic spirals, it is important to first investigate the structure of their Fourier spectra, or reciprocal space vectors, which can be obtained by the amplitude of the discrete Fourier transform (DFT) of the arrays. However, since spiral arrays are nonperiodic, a Brillouin zone cannot be rigorously defined. As a result, when comparing the diffraction patterns of different types of aperiodic spirals, it is important to adopt an approach that guarantees the homogeneous sampling of their aperiodic spectral features. This can be done by restricting their reciprocal space vectors within to the so-called "pseudo-Brillouin zones",[7] which contain spatial frequencies in the compact interval $\pm 1/\Delta$, being Δ the average interparticle separation.[30,31] The calculated pseudo-Brillouin zones of the three types of nanofabricated spirals are shown in Figures 1g−i. Diffuse spectra (i.e., absence of Bragg peaks) with rotational symmetry (i.e., scattering rings) are clearly observed for all the spirals in Figure 1. While the g-spiral features a broad and central scattering ring (Figure 1g), the more inhomogeneous structure of the α_2 (Figure 1b,e) and the α_1 (Figure 1c,f) spirals is reflected by the presence of multiple scattering rings embedded in a diffuse

dx.doi.org/10.1021/nl2003736 |Nano Lett. XXXX, XXX, 000–000

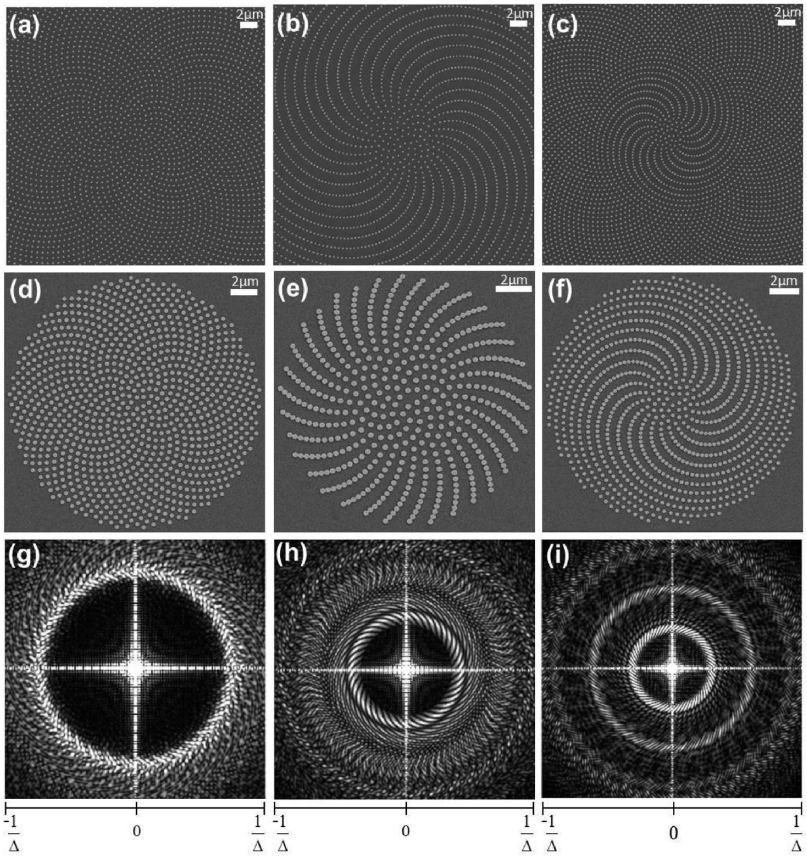

Figure 1. SEM micrographs of (a) g-spiral, (b) α_2-spiral, (c) α_1-spiral Au nanoparticle array. The arrays have 27 778 particles with a diameter of 200 nm. SEM micrographs of (d) g-spiral, (e) α_2-spiral, (f) α_1-spiral Au nanoparticle arrays containing 1000 particles with a diameter of 200 nm. (g–i) Calculated pseudo-Brillouin zones of the (d) g-spiral, (e) α_2-spiral, (f) α_1-spiral arrays where Δ represents the average center-to-center particle separation.

background of weaker intensity. The circular symmetry of the reciprocal space of aperiodic spirals has direct implications on their diffractive properties. This can already be appreciated within standard Fourier optics, neglecting near-field (quasi-static) interactions among neighboring particles. Under these conditions, well-satisfied by the choice of samples parameters, normal incidence radiation of wavelength λ is diffracted into the plane of the arrays when its longitudinal wavevector component vanishes, that is, $k_z = 0$. This requirement is equivalent to the well-known Rayleigh cutoff condition that determines the propagation of the first diffractive order of a periodic grating on its planar surface.[32] The Rayleigh condition depends on wavelength λ and on the transverse spatial frequencies ν_x and ν_y of the diffracting element, according to

$$k_z = 2\pi\sqrt{(1/\lambda)^2 - \nu_x^2 - \nu_y^2} = 0 \qquad (3)$$

Equation 3 is satisfied on a circle of radius $1/\lambda$ in reciprocal space, and therefore structures with circularly symmetric Fourier space satisfy the Rayleigh cutoff condition irrespective of the polarization of the incident field, strongly diffracting normal incident radiation into evanescent grating modes. We say that the resonant condition expressed by eq 3 induces "planar diffraction". It is important to notice that, differently from periodic crystals and quasicrystals with finite-order rotational symmetries, aperiodic spirals satisfy the condition for planar diffraction over a range of wavelengths uniquely determined by the number and

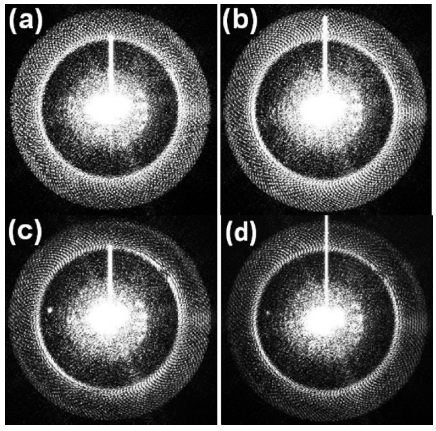

Figure 2. Experimentally measured far-field diffraction spectra of a g-spiral (8000 particles) illuminated by an HeNe laser at 633 nm under different conditions: (a) unpolarized, (b) circular polarized, (c) linear polarized (0°), and (d) linear polarized light (60°). We observe that the vertical line common to all the diffraction spectra is an experimental artifact introduced by the CCD camera.

the width of the scattering rings in their reciprocal space. The multiband/broadband polarization-insensitive planar diffraction of aperiodic spirals is therefore a highly desirable property for the engineering of a variety of device applications that require increasing photonic-plasmonic coupling on planar optical chips.

dx.doi.org/10.1021/nl2003736 |*Nano Lett.* XXXX, XXX, 000–000

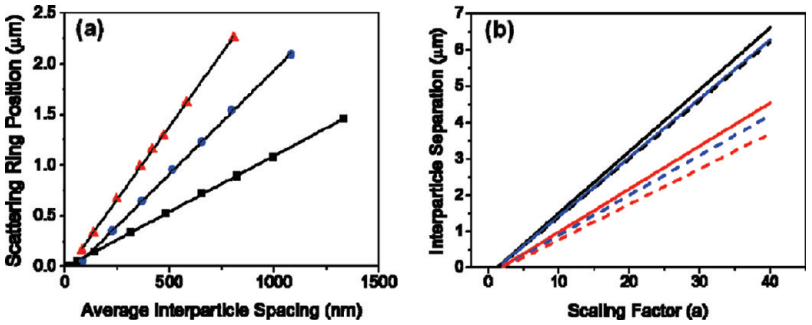

Figure 3. (a) Inverse of the scattering ring radius ν in the reciprocal space as a function of the average interparticle spacing for a g-spiral (black), α_1-spiral (blue), and α_2-spiral (red). (b) Calculated average (solid lines) and minimum (dotted lines) edge-to-edge interparticle separation as a function of the scaling factor for the g-spiral (black), α_1-spiral (blue), and α_2-spiral (red). All the arrays considered in this analysis contain 8000 particles.

In order to experimentally demonstrate polarization-insensitive circular scattering from aperiodic spirals, we directly measured their Fraunhofer far-field intensity (i.e., the diffraction pattern) using different polarizations at normal incidence. In this paper, we show the results on the g-spiral (Figure 2) because similar far-field patterns were also obtained for the α_1 and α_2-spirals (see Figure 1g−i). The diffraction spectra reported in Figure 2a−d were measured on a g-spiral with 8000 Au nanoparticles, and an average edge-to-edge interparticle separation of 312 nm. The diffraction far-field patterns were observed using a HeNe laser (λ = 633 nm) source. The transmitted light was collected with a 60× objective (NA = 0.85), collimated, and focused by lenses with focal lengths of 150 and 100 mm onto a CCD camera (Apogee Alta U4000 Camera w/KAI-4022 CCD). The polarization of the incident beam was controlled by appropriate configurations of quarter and half-wave plates in the beam path. Figure 2a shows the measured Fraunhofer far-field of the g-spiral using unpolarized illumination, which agrees very well with the calculated far-field pattern shown in Figure 1g. The incident polarization was also varied from circular to linear (along two orthogonal axes) in order to demonstrate the robustness of circular scattering to the polarization conditions, as demonstrated in Figures 2b−d.

It is important to note that simple linear scaling laws determine the frequency of planar diffraction in circularly symmetric aperiodic spirals. In Figure 3a, we plot the calculated spectral position (i.e., in units of inverse spatial frequency) of the center of the first scattering ring in Fourier space for each type of spiral, as a function of the average interparticle separation. We notice in Figure 3a that the scattering ring position of the g-spiral scales nearly one to one with the average interparticle separation (slope approximately equal to 1), a result that is in agreement with what reported by Pollard et al.[28] for dielectric spirals. On the other hand, for the α_1 and α_2-spirals the scattering ring positions scale more rapidly with the interparticle separations, according to linear relations with increasing slopes (i.e., equal to approximately 2.05 and 2.89, respectively). In Figure 3b, we show the simple linear relations that we connect the average interparticle separation in the spirals with the corresponding scaling factors. The relations shown in Figure 3 enable the engineering of planar diffraction effects in circularly symmetric aperiodic spirals.

Dark-Field Scattering Analysis. Using dark-field microscopy in the visible spectral range, we investigated the scattering properties of plasmonic spiral arrays fabricated with different interparticle separations. For this analysis, the structures consisted of g-spirals with interparticle separations ranging from 312 to 568 nm, and α_2-spirals with separations from 220 to 430 nm. The results obtained on α_2-spirals are very similar to the ones on α_1-spirals, which are therefore not shown here. Transmission scattering measurements were performed under incoherent white-light illumination using a dark-field microscope setup (Olympus, IX71) with a 10× long-working distance objective (NA = 0.3) coupled to a grating spectrometer and CCD detector (Andor, Shamrock 750). The incident angle of illumination was approximately 15° with respect to the normal to the array plane, and spatial filtering at the CCD detector was used for background noise reduction. The dark-field images of the samples where collected in the same microscope configuration by a CCD digital camera (Media Cybernetics Evolution VF). All the scattering spectra were background corrected by subtraction of the scattering signal from an equal-size, unpatterned area adjacent to each spiral. The scattering spectra were additionally corrected by the division with respect to the normalized emission line shape of the excitation lamp (tungsten halogen bulb). In Figure 4a,b, we show the corrected dark-field scattering spectra measured on g-spirals and α_2-spirals, respectively. We remark that the g-spiral, while lacking global periodicity, is "the most regular" among the aperiodic spirals and the measured scattering bands significantly red shift with increasing interparticle separation. This behavior is analogous to what observed in the case of periodic plasmonic gratings,[33−35] where scattering peaks red shift due to the coherent contribution of diffraction (i.e., radiative) coupling. However, for all spirals, we found that the scattering spectra are significantly affected by higher order scattering modes developing in the 500−600 nm spectral range. These modes, which are weakly radiative in regular (i.e., periodic) media, are efficiently enhanced at multiple frequencies in structures with "broken symmetry" such as the aperiodic spirals.[36,37] The red shift of the scattering bands is not observed for the more structurally inhomogeneous α_2-spirals because the dipolar modes are mostly outside our experimental range, as evident from the calculated cross sections shown in Figure 4c,d. However, the spectral mixing of dipolar modes with higher order ones makes the α_2-spirals relatively insensitive to increasing interparticle separation (Figure 4d). The complex interplay between dipolar and higher order scattering modes has been previously observed in multiscale aperiodic arrays with diffuse Fourier spectra generated by deterministic inflation rules.[3]

To support the interpretation of our experimental results, we used the rigorous multiparticle GMT for the electromagnetic modeling of light scattering. Being formulated in the complex domain, the GMT can be conveniently applied to study plasmonic

dx.doi.org/10.1021/nl2003736 |*Nano Lett.* XXXX, XXX, 000–000

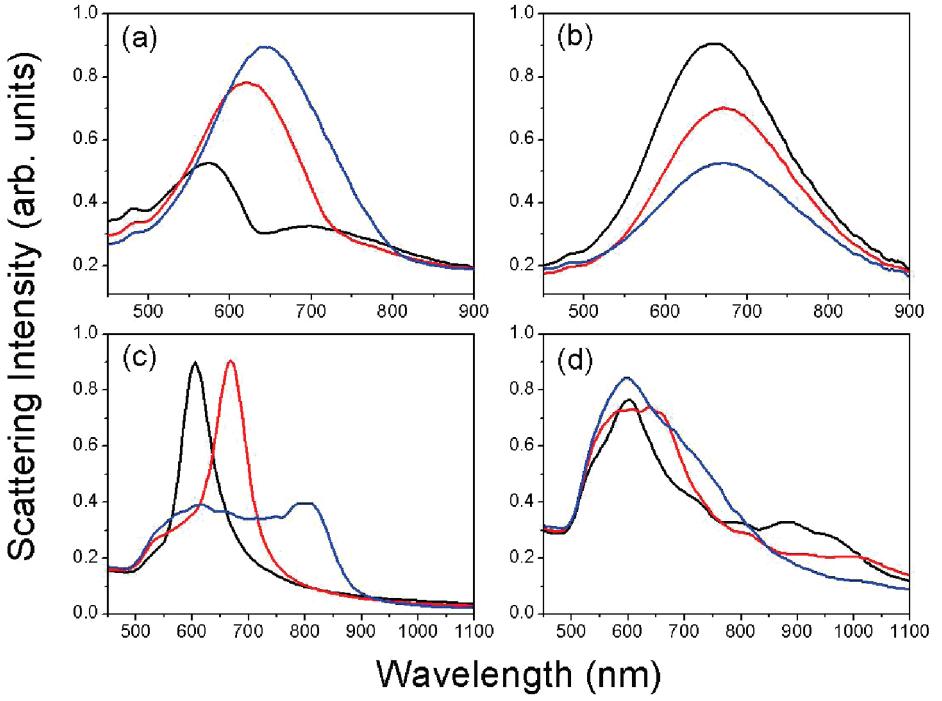

Figure 4. Measured dark-field scattering spectra of (a) g-spiral with average interparticle separations d equal to 312 nm (black, 27 778 particles), 398 nm (blue, 20 408 particles), and 568 nm (red, 12 346 particles). (b) α_2-spiral with average interparticle separations d equal to 220 nm (black, 27 778 particles), 290 nm (blue, 20 408 particles), 430 nm (red, 12 346 particles). (c) GMT calculated scattering efficiency of (c) g-spiral (1 500 particles) and (d) α_2-spiral (1 500 particles) with average interparticle separations matching values in (a) and (b), respectively.

structures with realistic material losses. In our calculations, the optical dispersion of Au nanoparticles was obtained by a spline interpolation of the Johnson and Christy dispersion data for Au.[38] Although the validity of the GMT calculation method is limited to clusters of spherical objects, it yields the full analytical solution of multiparticle scattering problems, efficiently providing valuable physical insights into the complex behavior of aperiodic systems.[3,39,40] Figure 4c,d shows the GMT-calculated scattering efficiencies obtained under linearly polarized excitation at normal incidence on spiral arrays of 1500 nanospheres, 200 nm in radius. The calculated spectra correspond to g-spirals and the α_2-spirals, respectively. In order to more clearly visualize the respective contributions of the dipolar versus higher order scattering modes, we have shown the calculated scattering spectra on a slightly larger wavelength range (i.e., from 450–1100 nm) compared to the corresponding experimental data, which are limited by the detector sensitivity range. These calculations fully confirm the important role played by radiative coupling effects in determining the scattering resonances of the dipolar modes of g-spirals, which significantly red shift with increasing interparticle separations. We notice that the calculated dipolar resonances of the g-spirals are substantially narrower than what experimentally measured (Figure 4a). This discrepancy is attributed to the combined effects of the noncollinear nature of the dark-field excitation (limiting frequency resolution) and to the presence of the quartz substrate preventing efficient phase matching at the superstratum.[3] On the other hand, no appreciable shifts and much broader scattering resonances are observed for the more inhomogeneous α_2-spirals (Figure 4d) due to the contribution of higher order modes appearing in the visible spectral range, which is in agreement with the experimental results shown in Figure 4b.

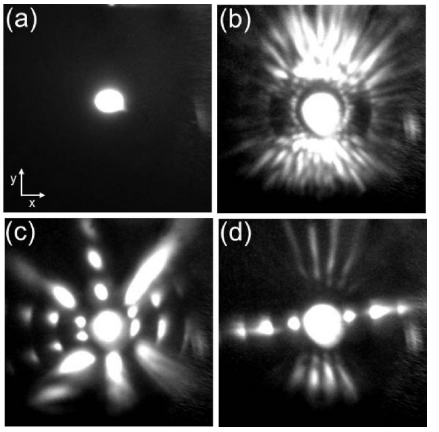

Figure 5. CCD image of light emission from a DCM dye layer (100 nm thick) deposited onto (a) homogeneous quartz substrate (b) dye emission from scattered light of α_2-spiral (27 778 particles) with laser positioned at the center of the spiral. (c,d) Dye emission from scattered light of α_2-spiral with laser positioned off center of the spiral. The peak emission wavelength was 640 nm and the pump laser wavelength was 480 nm. Samples are pumped with the same power of 30 mW.

A particularly attractive feature of these scattering resonances, which follows from the circular symmetry of the Fourier space, relies on the possibility of polarization-insensitive, planar diffraction of incident radiation at multiple frequencies, thus enhancing light-matter coupling phenomena in thin-film structures. In order to better visualize the effect of planar diffraction originating from the local spatial frequencies on the spirals surface, we have directly imaged the fluorescence of a thin dye polymer layer coated on top of the aperiodic spirals. For this experiment, we

dx.doi.org/10.1021/nl2003736 |*Nano Lett.* XXXX, XXX, 000–000

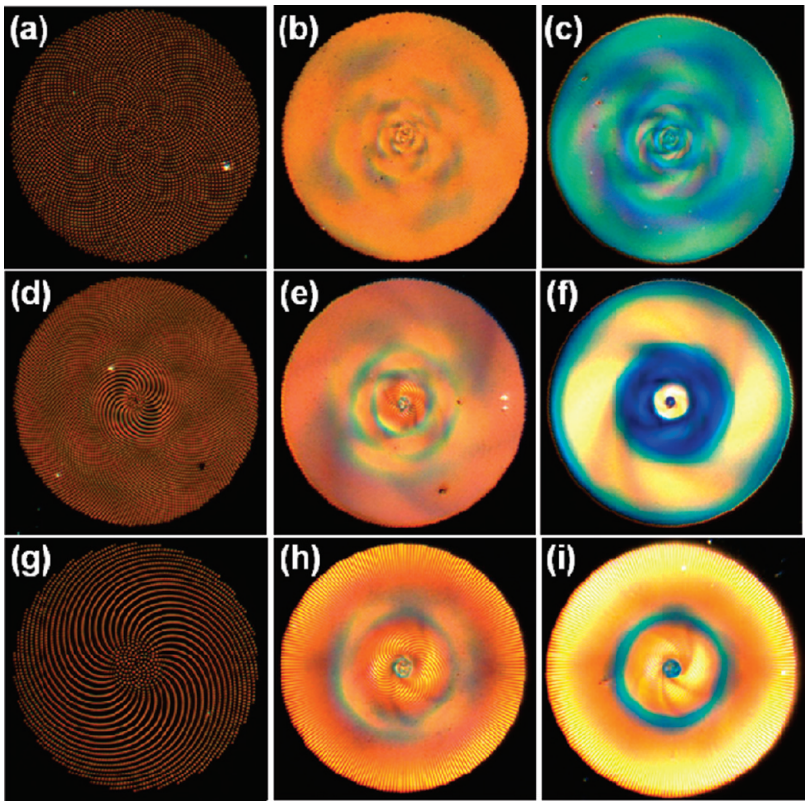

Figure 6. Dark-field microscopy images of plasmonic spirals on quartz substrates. The samples consist of g-spirals (a−c), α_1-spirals (d−f), and α_2-spirals (g−i) of varying (average) interparticle separations, as follows: (a) 1240, (b) 565, (c) 310, (d) 918 (e) 418, (f) 242, (g) 906, (h) 298, and (i) 208 nm. All the nanoparticles are Au nanocylinders of 200 nm diameter and 30 nm height.

prepared a dye polymer solution by dissolving common laser dye molecules of DCM (Exciton Inc.) in toluene. The dilute solution was then mixed with PMMA, spun onto samples and cured, resulting in 100 nm thick films of laser dye doped PMMA. This particular laser dye has maximum absorption at 480 nm and an emission peak at 640 nm, which overlaps the scattering resonances of α_2-spirals shown in Figure 4b. The sample was pumped by positioning the laser spot at different locations onto the doped PMMA substrate at normal incidence (focused through a 10× objective) with a laser diode at 480 nm and the emitted light was collected in transmission configuration through the substrate using a lens of 100 mm focal length and imaged by a CCD camera. In order to capture only the emission patterns, the pump laser light was blocked by a 514 nm high-pass filter. An identically prepared emitting layer was also coated on unpatterned quartz for reference. Figure 5 shows the CCD images of the fluorescence collected in transmission through the reference sample when pumped at different locations on its surface (Figure 5a) and through a representative α_2-spiral, respectively. The data in Figure 5b−d visibly demonstrate the spreading of the fluorescence signal in the plane of the spiral array, where a significant fraction of the intensity is emitted along multiple directions when the sample is symmetrically pumped through its center (Figure 5b). Additionally, we also observed that the angular distribution of the radiation changes dramatically when the position of the laser pumping spot is slightly misplaced (in the x-direction) from the center of the sample by approximately 25 μm in Figure 5c and 50 μm in Figure 5d. This effect is due to the excitation of different spatial frequencies on the surface of the sample, which translates into vastly different angular spectra. On the other hand, when pumping the dye-doped reference sample (Figure 5a), the emission intensity remains well-confined within the pumping spot size of approximately 50 μm. The effect reported in Figure 5 is a direct consequence of the inhomogeneous distribution of local spatial frequencies associated to the surface of aperiodic spirals with circularly symmetric Fourier space, and will be further analyzed in the next section.

Circular Light Scattering in Aperiodic Spirals. The scattering resonances of aperiodic spirals most strikingly manifest their characteristic circular symmetry when imaged in dark-field mode under white-light illumination. In Figure 6, we have imaged the dark-field scattered intensity collected from the three types of aperiodic spirals fabricated with three distinct values of scaling factors, corresponding to different interparticle separations. Each spiral is fabricated with a constant array diameter of 100 μm (number of particles ranging between 8264 to 33 058). In particular, Figure 6a−c corresponds to g-spirals, Figure 6d−f to α_1-spirals, and Figure 6 (g−i) to α_2-spirals of decreasing interparticle separations from left to right. We notice in Figure 6 that the dark-field images exhibit highly inhomogeneous spatial distributions of different chromatic components that critically depend on the spiral geometry as well as the minimum interparticle separation. When the interparticle separation is decreased, diffractive coupling effects become more significant and fascinating structural resonances are observed in Figure 6. Interestingly, we discovered that the α_1- and α_2-spirals (Figure 6f,i) display scattered patterns with a remarkable degree of circular symmetry at the wavelengths matching the local spatial frequencies of the structures. When illuminated by white light, each scattering ring efficiently diffract light of different wavelengths in

dx.doi.org/10.1021/nl2003736 |*Nano Lett.* XXXX, XXX, 000–000

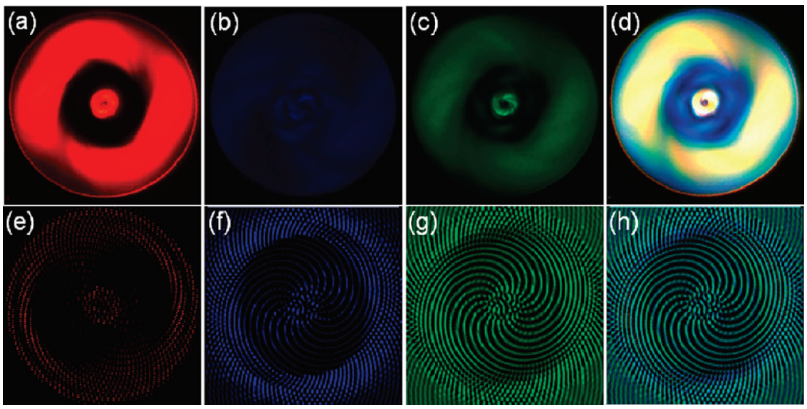

Figure 7. (a−c) Wavelength filtered ((a) 585 nm long pass, (b) 360−460 nm band-pass and (c) 490 nm −560 nm band-pass) dark-field images of an α_1-spiral with particle diameter of 200 nm and average separation of 242 nm. (d) Dark-field image under white light illumination and unfiltered detection. (e−g) GMT calculated electric field amplitude at (f) 475 nm, (g) 510 nm, (e) 650 nm, and (h) incoherent sum (intensity addition) of the three scattering profiles e-g. All simulated arrays have 1500 particles with a diameter of 200 nm.

the array plane, as observed in Figure 5. This effect is less pronounced in the g-spirals due to their higher degree of structural uniformity manifested by the presence of only one broad scattering ring in Fourier space. To further understand the physical nature of these complex structural resonances, we utilized band-pass filters to collect dark-field scattering images at specific wavelengths, as shown in Figure 7a−c for the α_1-spiral. We notice that similar results can be obtained for all the structures (as shown in Figure 6), and therefore we limit the following analysis to the α_1-spiral for convenience. The dark-field images of Figure 7a−c were collected in the same configuration as in Figure 6, using red, blue, and green band-pass filters in front of the CCD camera. In Figure 7d, we show the unfiltered dark-field image of the same spiral. We notice that the chromatic components shown in Figure 7a,c share similar spatial patterns and give rise, when superimposed, to the outer diffraction corona observed in Figure 7d. On the other hand, the more homogeneous intensity distribution of the scattered component in Figure 7b is responsible for the formation of the inner diffraction corona observed in Figure 7d. These data experimentally demonstrate that the distinctive structure of spatial frequencies associated to the inhomogeneous particle arrangements of the α_1- and α_2-spirals diffract incident radiation into a number of circularly symmetry scattering resonances. All the previous experimental results are consistent with GMT calculations of the near-field intensity distributions in the plane of the array for the corresponding spirals. The simulations have been performed under a linearly polarized plane wave excitation at normal incidence. We show in Figure 7(e−g) the calculated electric field magnitudes for individual wavelengths of λ_R = 650 nm (e), λ_B = 475 nm (f), λ_G = 510 nm (g), while in Figure 7h we show the superposition of the intensity patterns corresponding to the three previous wavelengths.[3] All the calculations refer to an α_1-spiral array with 1500 particles of 200 nm diameter and average interparticle separation of 242 nm. The qualitative agreement between single color and polychromatic scattering data and dark-field images is only limited by our computational power that forces us to restrict the simulation area to ∼1/5 of the experimental array size. However, we note that the GMT simulations well capture the physical picture behind the formation of dark-field scattering images in these large systems and indicate that these effects are robust with respect to the total number of particles in the spirals.

Angular Momentum of Light in Aperiodic Spirals. We observe that the dark-field images of aperiodic spirals shown in Figures 6 and 7 are consistent with the formation of a vortex-like intensity distribution spiraling toward the center of the images. In order to rigorously demonstrate that circularly symmetric scattering resonances in aperiodic spirals can indeed carry orbital angular momentum giving rise to polarization vortices, we performed a more detailed GMT analysis of the scattered fields. In particular, we calculated the spatial distributions of the scattered electric field intensity corresponding to different vertical positions measured from the array plane, as well as the azimuthal components of the electromagnetic linear momentum, which directly conveys information of the angular momentum.[41] We performed this analysis on an α_2-spiral with geometric parameters as in Figures 5 and 6i, because this type of spiral has been previously investigated in relation to planar diffraction, as shown in Figure 5. For this reason, we carried out our calculations at 480 and 650 nm, previously utilized as pumping and fluorescent wavelengths in the fluorescence diffraction experiment. In what follows, only the results corresponding to the 650 nm excitation will be shown in the interest of conciseness. However, we notice that a similar physical picture also emerged from the simulations performed at 480 nm, shown in the Supporting Information. In Figure 8a−c, we plot the scattered intensity profiles calculated at 1, 3, and 10 μm from the plane of the array, and homogeneously excited at normal incidence by a plane-wave. It is evident from Figure 8a−c that the scattered intensity patterns rotate clockwise as they propagate away from the array plane. The interaction of the incident plane wave with the spiral structures transfers net orbital momentum to the scattered radiation. This effect is demonstrated in Figures 8d where we plot the azimuthal component p_ϕ of the linear electromagnetic momentum density. The linear momentum density is obtained by calculating the ratio of the time-averaged Poynting vector S with the square of the free-space velocity of light.[41] It is known that the p_ϕ component of the linear momentum density is directly related to the angular momentum density of a free beam that propagate along the vertical z axis (the spiral arrays lie in the horizontal x-y pane) by the linear relation[41]

$$J_z = rp_\phi \tag{4}$$

dx.doi.org/10.1021/nl2003736 |Nano Lett. XXXX, XXX, 000–000

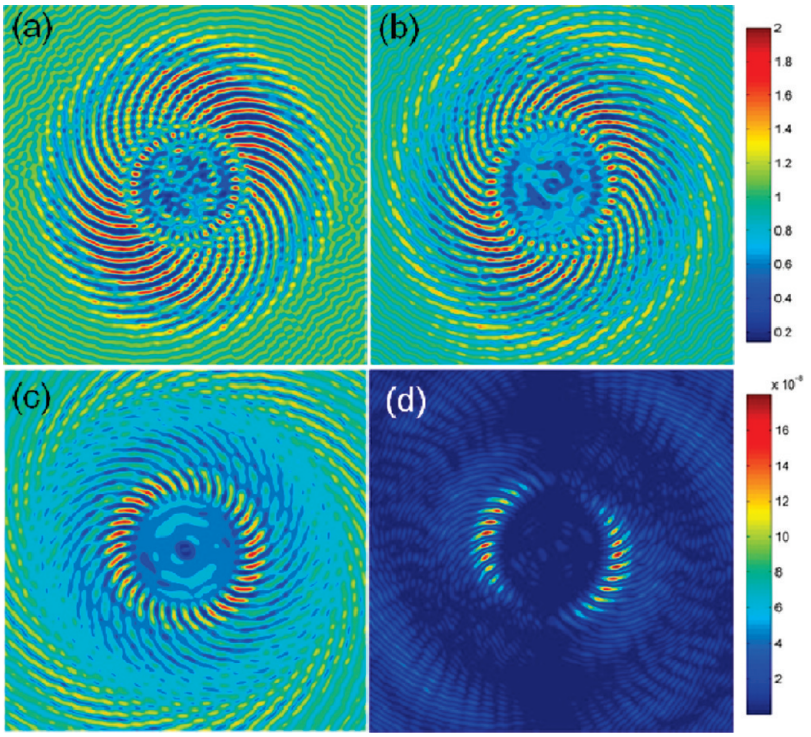

Figure 8. Analytical GMT simulations of an α_2-spiral. Simulation consists of 1500 Au spheres of diameter 200 nm excited with a linearly polarized plane wave λ = 650 nm. Scattered intensity profiles calculated at (a) 1, (b) 3, and (c) 10 μm from the plane of the array. (d) Magnitude of the azimuthal-component of the linear momentum density of the scattered electromagnetic field at 10 μm above (time-average Poynting vector normalized to c^2).

where r is the position vector. The results shown in Figures 8d provide a rigorous justification to the angular momentum transfer associated to the excitation of the circularly symmetric scattering resonances in nanoplasmonic spirals. It is worth mentioning that phaseplates with spiral patterns have been previously utilized for the generation of free-space Lagure Gaussian modes at millimeter-wave frequencies.[42] No prior reports, to the best of our knowledge, of compact plasmonic nanostructures capable of encoding orbital angular momentum at optical frequencies onto a transmitted plane wave have been reported. The engineering of optical vortices in miniature-size chips is another exciting feature of aperiodic nanospirals that can result in compact polarization devices for on-chip nanoplasmonics and optical trapping applications.

Conclusions. In conclusion, we have studied the scattering properties of the three main types of deterministic aperiodic spiral arrays of Au nanoparticles and performed experimental dark-field scattering, imaging, and fluorescence spectroscopy in partnership with rigorous electrodynamics calculations. We studied circular symmetry in continuous Fourier space of Vogel's spirals and demonstrated polarization-insensitive planar diffraction. Moreover, we have shown that far-field diffractive coupling in these structures leads to the formation of scattering resonances with circular symmetry and characteristic vortex behavior carrying orbital angular momentum. We believe that the engineering of plasmonic nanoparticle arrays with aperiodic spiral geometry can lead to the fabrication of novel optical devices that benefit from polarization insensitive, enhanced light-matter coupling on planar surfaces, such as thin-film solar cells, plasmonic photodetectors, optical biosensors, and novel polarization devices.

■ ASSOCIATED CONTENT

Supporting Information. Additional figure. This material is available free of charge via the Internet at http://pubs.acs.org.

■ AUTHOR INFORMATION

Corresponding Author
*E-mail: dalnegro@bu.edu.

■ ACKNOWLEDGMENT

This work was supported by the Air Force program "Deterministic Aperiodic Structures for On-chip Nanophotonic and Nanoplasmonic Device Applications" under Award FA9550-10-1-0019, and by the NSF Career Award No. ECCS-0846651. The authors thank Dr. Heeso Noh for helpful discussions.

■ REFERENCES

(1) Dal Negro, L.; Feng, N. *Opt. Express* **2007**, *15* (22), 14396.
(2) Dal Negro, L.; Feng, N.; Gopinath, A. *J. Opt. A: Pure Appl. Opt.* **2008**, No. 10, 064013.
(3) Gopinath, A; Boriskina, S; Feng, N; Reinhard, B. M.; Dal Negro, L. *Nano Lett.* **2008**, No. 8, 2423.
(4) Luck, J. M. *Phys. Rev. B.* **1989**, No. 39, 5834.
(5) Barber, E. M. *Aperiodic Structures in Condensed Matter, Fundamentals and Applications*; CRC Press: Boca Raton, FL, 2009.
(6) Steurer, W.; Sutter-Widmer, D. *J. Phys. D: Appl. Phys.* **2007**, No. 40, R229.
(7) Janot, C. *Quasicrystals: a primer*; Clarendon Press: Oxford, 1992.
(8) Senechal, M. *Quasicrystals and geometry*; Cambridge University Press: New York, 1996.

dx.doi.org/10.1021/nl2003736 |*Nano Lett.* XXXX, XXX, 000–000

(9) Vasconcelos, M. S.; Albuquerque, E. L. *Phys. Rev. B* **1998**, No. 57, 2826.
(10) Matsui, T.; Agrawal, A.; Nahata, A.; Vardeny, Z. V. *Nature* **2007**, No. 446, 517.
(11) Huang, F. M.; Kao, T. S.; Fedotov, V. A.; Chen, Y.; Zheludev, N. I. *Nano Lett.* **2008**, No. 8, 2469.
(12) Huang, F. M.; Zheludev, N. I.; Chen, Y.; Javier Garcia de Abajo, F. *Appl. Phys. Lett.* **2007**, No. 90, 091119.
(13) Pacifici, D.; Lezec, H. J.; Sweatlock, L. A.; Walters, R. J.; Atwater, H. A. *Opt. Express* **2008**, No. 16, 9222.
(14) Florescu, M.; Torquato, S; Steinhardt, P. J. *Proc. Natl. Acad. Sci. U.S.A.* **2009**, *49* (106), 20658.
(15) Zachary, C. E.; Torquato, S. *J. Stat. Mech.: Theory Exp.* **2009**, No. 12, P12015.
(16) Quinten, M.; Kreibig, U. *Appl. Opt.* **1993**, No. 32, 6173.
(17) Mackowski, D. W. *J. Opt. Soc. Am. A* **1994**, No. 11, 2851.
(18) Xu, Y. L. *Appl. Opt.* **1995**, No. 34, 4573.
(19) Kreibig, U.; Vollmer, M. *Optical properties of metal clusters*; Springer-Verlag: New York, 1995.
(20) Bohren, C. F.; Huffman, D. R. *Absorption and scattering of light by small particles*; Wiley-VCH: New York, 1998.
(21) Vogel, H. *Mathematical Biosciences* **1979**, No. 44, 179.
(22) Mitchison, G. J. *Science* **1977**, *196* (4287), 270.
(23) Naylor, M. *Mathematics Magazine* **2002**.
(24) Ruelle, D. *Physica A* **1982**, No. 113, 619–623.
(25) Agrawal, A.; Kejalakshmy, N.; Chen, J.; Rahman, B. M. A.; Grattan, K. T. V. *Opt. Lett.* **2008**, No. 33, 2716.
(26) Agrawal, A.; Kejalakshmy, N.; Rahman, B. M. A.; Grattan, K. T. V. *Appl. Phys. B: Laser Opt.* **2010**, *4* (99), 717.
(27) Agrawal, A.; Kejalakshmy, N.; Rahman, B. M. A.; Grattan, K. T. V. *IEEE Photonics Technol. Lett.* **2009**, *22* (21), 1722.
(28) Pollard, M. E.; Parker, G. J. *Opt. Lett.* **2009**, No. 34, 2805–2807.
(29) Adam, J. A. *A mathematical nature walk*; Princeton University Press: Princeton, NJ, 2009.
(30) Forestiere, C.; Miano, G.; Rubinacci, G.; Dal Negro, L. *Phys. Rev. B* **2009**, No. 79, 085404.
(31) Forestiere, C.; Walsh, G. F.; Miano, G.; Dal Negro, L. *Opt. Express* **2009**, No. 17, 24288–24303.
(32) Fano, U. *J. Opt. Soc. Am.* **1941**, *3* (31), 213.
(33) Felidj, N.; Laurent, G.; Aubard, J.; Levi, G.; Hohenau, A.; Krenn, J.; Aussenegg, F. R. *J. Chem. Phys.* **2005**, No. 123, 221103.
(34) Meier, M.; Wokaun, A.; Liao, P. F. *J. Opt. Soc. Am. B* **1985**, No. 2, 931.
(35) Carron, K. T.; Fluhr, W.; Meier, M.; Wokaun, A.; Lehmann, H. W. *J. Opt. Soc. Am. B* **1986**, No. 3, 430.
(36) Hao, F.; Sonnefraud, Y.; Van Dorpe, P.; Maier, S. A.; Halas, N. J.; Nordlander, P. *Nano Lett.* **2008**, *11* (8), 3983.
(37) Kim, H; Park, J; Cho, S. W.; Lee, S. Y.; Kang, M.; Lee, B. *Nano Lett.* **2010**, *10* (2), 529–536.
(38) Johnson, P. B.; Christy, R. W. *Phys. Rev. B* **1972**, No. 6, 4370.
(39) Gopinath, A.; Boriskina, S.; Reinhard, B.; Dal Negro, L. *Opt. Express* **2009**, No. 17, 3741.
(40) Gopinath, A.; Boriskina, S.; Presamiri, R.; Ziegler, L.; Reihard, B. M.; Dal Negro, L. *Nano Lett.* **2009**, *11* (9), 3922.
(41) *Structured light and its applications*; Andrews, D. L., Ed.; Elsevier: New York, 2008.
(42) Turnbull, G. A.; Robertson, D. A.; Smith, G. M.; Allen, L.; Padgett, M. J. *Opt. Commun.* **1996**, No. 127, 183.

dx.doi.org/10.1021/nl2003736 |*Nano Lett.* XXXX, XXX, 000–000